Propulsion and Power Research 2020;9(1):75–86

http://ppr.buaa.edu.cn/

Propulsion and Power Research

www.sciencedirect.com

ORGINAL ARTICLE

Performance index improvement of a double-pipe cooler with MgO/water-ethylene glycol (50:50) nano-suspension

H. Arya[a,*], M.M. Sarafraz[b], O. Pourmehran[b], M. Arjomandi[b]

[a]*Centre for Energy Resource Engineering, Technical University of Denmark, Denmark*
[b]*School of Mechanical Engineering, University of Adelaide, South Australia, Australia*

Received 15 April 2018; accepted 24 May 2019
Available online 12 December 2019

KEYWORDS

Forced convective heat transfer;
Particulate fouling;
Heat exchanger;
Fouling;
Nanofluid

Abstract A series of tests was conducted to unlock the potential application of MgO/water-EG (ethylene glycol) nanofluids (NF) in a double-pipe heat exchanger (HEX). The overall heat transfer coefficient (HTC), the inlet temperature of the working fluid, the fluid pressure drop (FPD), friction factor (FF) and the hydraulic performance index of the NF within the HEX were experimentally measured. Fouling of nanoparticles (NPs) within the Hex was also studied and modelled using asymptotic particulate fouling model. Results showed that MgO NPs can enhance the HTC by 39% at $Re = 10{,}500$ and wt.% = 0.3 in the turbulent regime. Also, the presence of MgO NPs augmented the FF and the FPD values. The former was enhanced 33.8%, while the latter was augmented by 37% both at wt.% = 0.3 and at Reynolds number = 10,500. Results also revealed that the formation of porous particulate fouling layer on the internal wall of the inner tube creates a fouling thermal resistance which changes asymptotically with time. Overall, MgO/water-ethylene glycol shows a great potential to be used as a coolant within a HEX.

1. Introduction

Heat exchangers (HEXs) are essential tools in domestic and industrial processes [1], cooling systems and power cycles, providing conditions to transfer heat from a hot fluid to a cold working fluid in a confined space [2–10]. Depending on the application, there are different types of

*Corresponding author.
E-mail address: Hossein.arya.tk@gmail.com (H. Arya).
Peer review under responsibility of Beihang University.

Production and Hosting by Elsevier on behalf of KeAi

https://doi.org/10.1016/j.jppr.2019.05.001

HEX which are classified into several categories including solid-solid, solid-liquid and solid-gas (air-side) HEXs [11,12]. With the progress in high-temperature processes such as waste heat recovery, the improvement in the efficiency of the liquid-liquid HEXs has received a great attention. One way to improve the efficiency of a HEX is to apply the process intensification to the design and fabrication of the HEX. Process intensification is a chain of techniques and methods by which the rate of heat transfer within the HEX increases. Using the extended surface area such as fins or thermal conductivity-enhanced material are the common pathways to increase the thermal efficiency of the HEX [13−15].

Parallel to the above-mentioned techniques, an improvement in the thermo-physical properties of the coolant in the HEX is one passive technique to plausibly increase the efficiency of the HEX [4−6,8−10,16−20]. Nanofluids (NFs) are new engineered thermal fluids with enhanced thermo-physical properties such as thermal conductivity and density [21], which not only increase the heat transfer coefficient (HTC) but also facilitate the heat transport within the base fluid with micro-mechanisms such as thermophoresis and Brownian motion [22]. A NF in comparison with the micro-fluids offers the low fluid pressure drop (FPD) and FF values, which in turn decrease the pumping power as well. Such advantageous features have been a driver for heat transfer experts to make effort for utilising the NFs in advanced thermal engineering systems and other specific areas such as biomechanics and microfluidics systems [23−27] and medical sciences [28,29]. Following section is a literature review conducting on the state-of-the-art studies on the enhancement of the heat transfer and thermal performance of the NFs.

2. Literature review

HEXs are designed and implemented depending on their applications, type of the working fluid and the space availability. Therefore, a literature review was conducted on the application of the NFs in various configurations of the HEXs including micro/compact, plate and double pipe.

The compact and the micro HEXs are two efficient types of the HEXs which provide superior HTC and sufficient residence time for the heat transfer, however, the FPD value in these systems is very high, which limits their applications. However, the plate HEX is one common type of HEX with wide applications in car cooling systems, lab-scale and plant-scale processes and the refrigeration systems. Plate HEXs offer high surface area and large HTC and also high FPD value. Therefore, many experiments have been conducted to assess the thermal performance of the plate HEXs. For example, in a study performed by Z.J. Luan et al. [30], they found a solution for the intensification of heat transfer rate within the HEX. They designed a novel configuration for the plate HEX and experimentally demonstrated that the resistance of flow in the designed HEX is relatively smaller than the common chevron-type HEXs (by 50%). However, they found that there is a trade-off between flow resistance and HTC. They reported a decreased by 26% in the HTC, which significantly decreased the thermal performance of the plate HEX. Also, thermal performance of the HEX was found to be a function of physical properties of coolant in the HEX. Lee et al. [31] assessed the thermal performance and heat transfer in a sinusoidal form of a plate HEX for a low-temperature application. They experimentally measured the HTC of water together with the FPD of the system. It was concluded that the plate HEX performance was poor due to the low mass flux of refrigerant. They also concluded that, the value for the FPD in water-side is the highest, while the HTC was the lowest at refrigerant-side due to the formation of vapor and two-phase flow. The thermal performance of the HEX was attributed to the thermo-physical properties of the coolant as well. Such findings were later confirmed by Peyghambarzadeh et al. [32−34].

Recently, NFs have been nominated to be used inside the HEXs to enhance the thermo-hydraulic performance of the HEX. For example, in a study Sarkar et al. [35] demonstrated that by using hybrid NF in a HEX system, the HTC value was enhanced by 39.1%. Similarly, Vinod et al. [36] showed that Fe_2O_3, Al_2O_3 and CuO NPs in a “cellulous carboxymethyl” as a “generic base fluid” can promote the performance of the thermal systems. Kumar et al. [37] studied the energetic performance of a HEX cooled with a NF. They showed that utilising CeO_2/water and ZnO/water can improve the performance of the system. Similar results have been published somewhere else by Anoop et al. [38] and the same conclusion were drawn.

Conventional coolers such as double-pipe HEX are simple in design and can be employed in various processes such as energy production, waste heat recovery, pharmaceutical and chemical process, food, and gas industries. The FPD value in this type of HEX is not as high as the values recorded for the plate or brazed HEX. Moreover, residence time is sufficient for a great heat transfer between the annulus and the inner tube. When it comes to the application of NF within the double-pipe HEX, extensive studies can be found in the literature. For example, Chun et al. [39] conducted a set of experiments on the potential application of alumina NF in a double-pipe HEX under the laminar flow and at different operating parameters. They reported a 13% enhancement in the HTC for alumina NF. They also noticed that the HTC and Nusselt number do not follow the available correlations. Thus, they developed a new correlation for predicting the Nusselt number based on the Reynolds number. Zamzamian et al. [40] conducted a set of experiments to analyze the thermal performance of the HEX working with alumina/ethylene glycol and CuO/ethylene glycol NFs on HTC in a double pipe HEX. They reported that the HTC can be increased with the increase in the operating temperature and NP concentration. Both parameters increased the HTC by 26% for alumina and by 37% for CuO NF.

Khedkar et al. [41] experimentally measured the heat transfer properties of Titana/water NFs in concentric tube HEX as a coolant. The NFs were the mixture of water and Titana NPs. Results showed that the HTC is enhanced when NPs are used within the double pipe HEX. An enhancement of 14% was observed. No information was given on the FPD of the system. In a similar work performed by Akhtari et al. [42], the alumina-water NF heat transfer in a double-pipe HEX with laminar flow was investigated. Several parameters including cold and hot flow rates (FR), NF temperature and concentration were examined. The results demonstrated that the rate of heat transfer enhances by increasing the cold and hot volume FRs, as well as the concentration of particles and the temperature of NF at the inlet. The results showed that the HTC was enhanced by 13.2% over the base fluid. However, they did not study on the FPD and pumping power of the NFs.

According to the aforementioned literature, NFs can be utilized as a heat transfer fluid (HTF) for enhancing the thermal performance of the HEX. However, following challenges need to be addressed before NF can widely be commercialized within the heat exchanging devices: (1) The presence of NPs enhances the HTC; however, the amount of enhancement is different from NF to another NF. (2) The FPD augmentation and FF enhancement are drawbacks of the use of NFs in the HEXs. Recently MgO NPs have been identified as a potential nano-powder for increasing the thermal performance of various systems [43−46]. MgO NPs have anomalous thermal conductivity, which in turn can enhance the conduction heat transfer within the system [47]. However, in most of the studies, the base fluid was water which has a limited boiling temperature of 100 °C, thereby, limiting the application of the NF. Thus, in the present work, MgO NPs were dispersed in water-ethylene glycol (WEG) as the working fluid not only to improve the boiling temperature but also to enhance the thermal features of the base fluid. Thus, MgO/WEG was experimentally investigated in a double pipe HEX to assess the influence of different parameters such as FR of NF, inlet temperature of NF, mass fraction of NPs, on HTC, Nusselt number, FPD and FF of the system. Also, a dynamic study was conducted to measure the fouling thermal resistance of the HEX.

3. Experimental

3.1. Test rig

In Figure 1, a schematic illustration of the test rig is depicted. This setup consists of four general sections including hot loop in which NF was circulated, cold loop in which water was circulated, double pipe HEX and measurement instruments. NF and water were circulated in the loops with two centrifugal pumps manufactured by DAB Company with stainless steel impeller and body. Water and NF both were loaded inside two heavily-isolated tanks (with glass wool K4) as shown in green and red colour. Temperature and FR of water in the cold loop were set to 25 °C and 2 l/min, respectively. Notably, to set the temperature of water, a refrigeration system (R-134a) thermostat bath was used. The FR of the NF in the hot loop was controlled with a Flownetix 0−50 l/min ultrasonic flow controller connected to the data logger. Also, a by-pass loop was implemented to accurately control the FR of NF within the HEX. The FR of water was controlled with a simple rota-meter (it has not been shown in Figure 1). The NF pressure and temperature were measured upstream and downstream of the test section

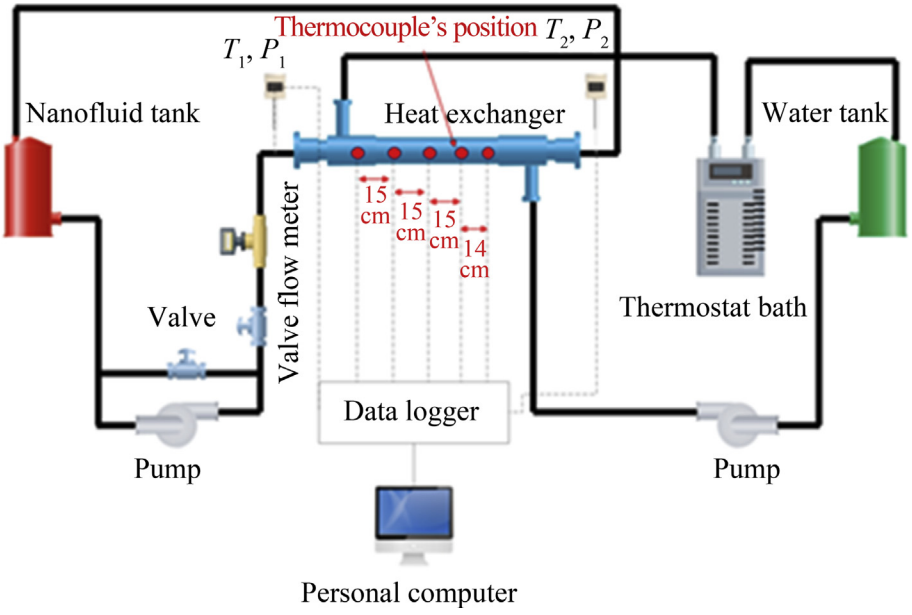

Figure 1 Experimental test rig used in the present work.

via two pressure transmitters (manufactured by Omega and accuracy of 1% of reading) and resistance temperature detector, (RTD) thermo-meters (manufactured by Omega and accuracy of 1% of reading). All thermocouples, thermometers and pressure transmitters were connected to a data logger manufactured by National Instruments (NI) to record the data continuously with data point reading frequency of 1 kHz. The data logger was connected to a personal computer using RS232 port with the setting of 8bit/parity: none.

The heart of the experimental setup was a double-pipe HEX consisting of two small copper tubes with the length of 90 cm and diameters of 6 mm and 12 mm, respectively. Water and NF were in counter-current contact within the HEX. NF was introduced into the inner tube and water was introduced into the annulus section. All other parts of the HEX were fabricated from copper heavily-isolated with glass wool. Experiments were conducted at various FRs, various mass fraction of NPs, and three different inlet temperature of NFs.

3.2. Preparation of the NFs

It is essential to uniformly disperse the NPs within the water ethylene glycol as the base fluid (WEG). This working fluid was selected because the physical properties of this working fluid are available and it has a wide application in cooling loops, car radiators and other cooling systems. This is usually done with adding a surfactant followed by using an ultrasonic homogeniser to crack the potential agglomerated NPs. Notably, agglomeration occurs due to the surface charge of the NPs resulting in the attraction of NPs to each other. This also affects the stability of NF. The higher, the amount of agglomeration is, the stability of NF becomes weaker and NPs deposit on the bottom of the vessel. To produce the NFs: (1) The NPs were scaled and dispersed in the base fluid. (2) A magnetic stirrer was used at 250 rpm to distribute the NPs within the base fluid. For a better dispersion, nonyl phenol ethoxilate was added to the nanofluid to reduce the rate of sedimentation. (3) Finally, a homogeniser was used at 400 Watt and 40 kHz to further disperse the NPs. (4) For the longest stability, the pH value of the NFs was regulated with a buffer liquid to set the zeta potential within the range of −20 mV to +20 mV. Table 1 tabulates the stability analysis results for NFs. The NF at wt.% = 0.3 possess the longest stability for 8 days.

The NFs showed a good stability (above a week). Also, the quality of NPs and dispersion procedure were also examined using scanning electron microscopy (SEM), particle size distribution analyser and transmission electron microscopy (TEM). As represented in Figure 2(a), the SEM image revealed the mean size of 45−50 nm, which was in accordance with the results of particle size test (Figure 2(b)). The TEM image, Figure 2(c), showed that NPs are dispersed uniformly within the liquid phase.

Table 1 The test conditions used for stabilizing the prepared NFs.

Mass fraction	Stirrer /rpm	Sonication /min	pH setting	Zeta potential/mV	Stability /day	Buffer /ml
0.1	250	10	7.6	−26	5	1.5
0.2	300	15	8.1	−31	7	2.5
0.3	400	15	8.7	−34	8	4

3.3. Thermo-physical properties of NF

Thermo-physical properties of the NF was measured with high-fidelity instruments and was compared with the equations represented in Table 2. The deviation value was also reported in Table 2. Density slightly increases by increasing the temperature (see Figure 3(a)). However, heat capacity (Figure 3(b)) and thermal conductivity (Figure 3(c)) enhance by increasing the temperature, while viscosity is suppressed by increasing the temperature (Figure 3(d)). Likewise, increase in the mass concentration of the particles resulted in the augmentation of the density, thermal conductivity and viscosity.

3.4. Formulation of the experiments

To obtain the HTC value, it is necessary to calculate the quantity of heat in the cold and hot loops, which are as follows:

$$Q_c = m_w \times C_{p,w} \times (T_{out} - T_{in}) \tag{1}$$

here, Q_c is the total amount for heat transfer occurring in the cold side, $C_{p,w}$ is the heat capacity of water at 25 °C. For the hot side:

$$Q_H = m_{nf} \times C_{p,nf} \times (T_{out} - T_{in}) \tag{2}$$

Q_H is the total heat exchanged in the hot side, which is also shown as Q_{nf} as well. Then, the arithmetic average of the heat exchanged between cold and hot sides is estimated with the following equation:

$$Q_{ave.} = \frac{Q_H + Q_c}{2} \tag{3}$$

And the overall HTC:

$$HTC \text{ or } U = \frac{Q_{ave.}}{A \times \Delta T_{LMTD}} \tag{4}$$

here, A is the circumference of the interior pipe of the HEX. Also, to facilitate evaluating the results, following non-dimensional groups were used including Nusselt and Reynolds and Prantdl numbers [50]:

$$Nu = \frac{h_{nf} \times D_{hydraulic}}{k_{nf}} \tag{5}$$

$$Re_{nf} = \frac{\rho_{nf} \times u_{nf} \times d_{hydraulic}}{\mu_{nf}} \tag{6}$$

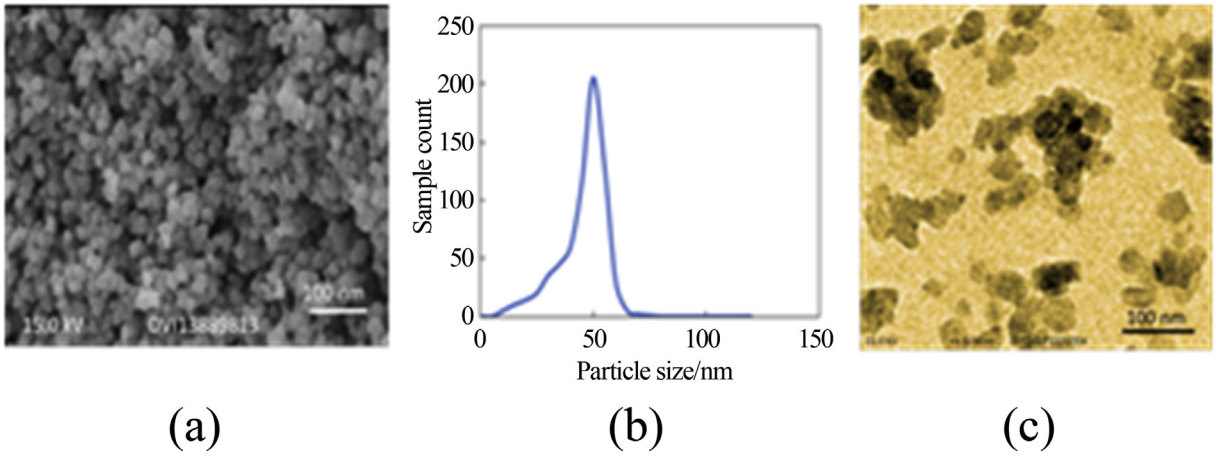

Figure 2 (a) Scanning electron microscopy, (b) particle size distribution, and (c) transmission electron microscopy image taken from the MgO/water-EG nanofluids [1].

Table 2 The equations utilized to calculate and compare the density, thermal conductivity, heat capacity and viscosity of the nanofluid [1].

	Correlation	Temperature /°C	A.A.D /%	Ref
Density[a]	$\rho_{nf} = \varphi \cdot \rho_p + (1-\varphi)\rho_{bf}$ $\varphi =$ volume fraction	20–100	3.8	[48]
Heat capacity[b]	$C_{p,nf} = \varphi \cdot C_{p,p} + (1-\varphi)C_{p,bf}$	20–100	2.9	
Viscosity[c]	$\mu_{nf} = A\left(\frac{1}{T}\right) - B$ $A = 20587\varphi^2 + 15857\varphi + 1078.3$ $B = -107.12\varphi^2 + 53.55\varphi + 2.8715$	20–100	4.9	[48]
Thermal conductivity[d]	$\frac{k_{nf}}{k_{bf}} = 0.8937 \times \left(1+\frac{\varphi}{100}\right)^{1.37} \times \left(1+\frac{T}{70}\right)^{0.277} \times \left(1+\frac{d}{150}\right)^{-0.0336} \times \frac{\alpha_p}{\alpha_{bf}}$ [49]	20–100	5.8	[48]

[a] $\rho_p = 3580$ kg/m^3, $\rho_{bf} = 1108$ kg/m^3.
[b] $C_{p,p} = 880$ J/(kg·K), $C_{p,bf} = 3400$ J/(kg·K).
[c] $\mu_{bf} = 2.8$ cp.
[d] $k_p = 112$ W/(m·K), $k_{bf} = 0.44$ W/(m·K).

$$Pr = \frac{c_{p,nf} \times \mu_{nf}}{k_{nf}} \tag{7}$$

h for the cold loop is calculated with the following equation:

$$\frac{h_w \times D_{hydraulic}}{k_w} = 0.2302 \times Re^{0.745} \times Pr^{0.4} \tag{8}$$

$D_{hydraulic}$ for the present research is $D_{hydraulic} = D_o - D_i$ which are 12.0 mm and 6.0 mm (nominal size), respectively. k_w, is thermal conductivity water-ethylene glycol (purity>99%). Likewise, for calculating h in the hot loop, following equation was implemented:

$$\frac{1}{U \text{ or } [HTC]} = \frac{1}{h_{nf}} + \frac{\delta}{k} + \frac{1}{h_w} \tag{9}$$

here, δ is the inner tube thickness which is 0.001 m, $k = 401$ W/(m·K) as HEX is copper-made, h_{nf} and h_w are attributed to HTC value (forced convective) of MgO/water-ethylene glycol nano-fluid and cold water, respectively.

To understand the influence of NP fouling in HEX, fouling thermal resistance parameter was defined as follows:

$$R_f(i) = \frac{1}{h_f}(t = t_i) - \frac{1}{h_c}(t = 0) \tag{10}$$

here, h is the HTC, c and f stand for clean surface and surface with fouling. h_f is HTC measured at time I when NPs deposited on the surface and h_c is HTC when surface is clean (at initial time of the experiments when $t = 0$). Likewise, R_f is the thermal fouling resistance of the NPs on the surface of inner tube of HEX. Using energy balance, a heat loss of 9.5% was calculated using Eq. (11):

$$Q_{nf} = Q_w + Q_{heat\ loss} \tag{11}$$

here, Q_{nf} and Q_w are obtained with Eqs. (1) and (2).

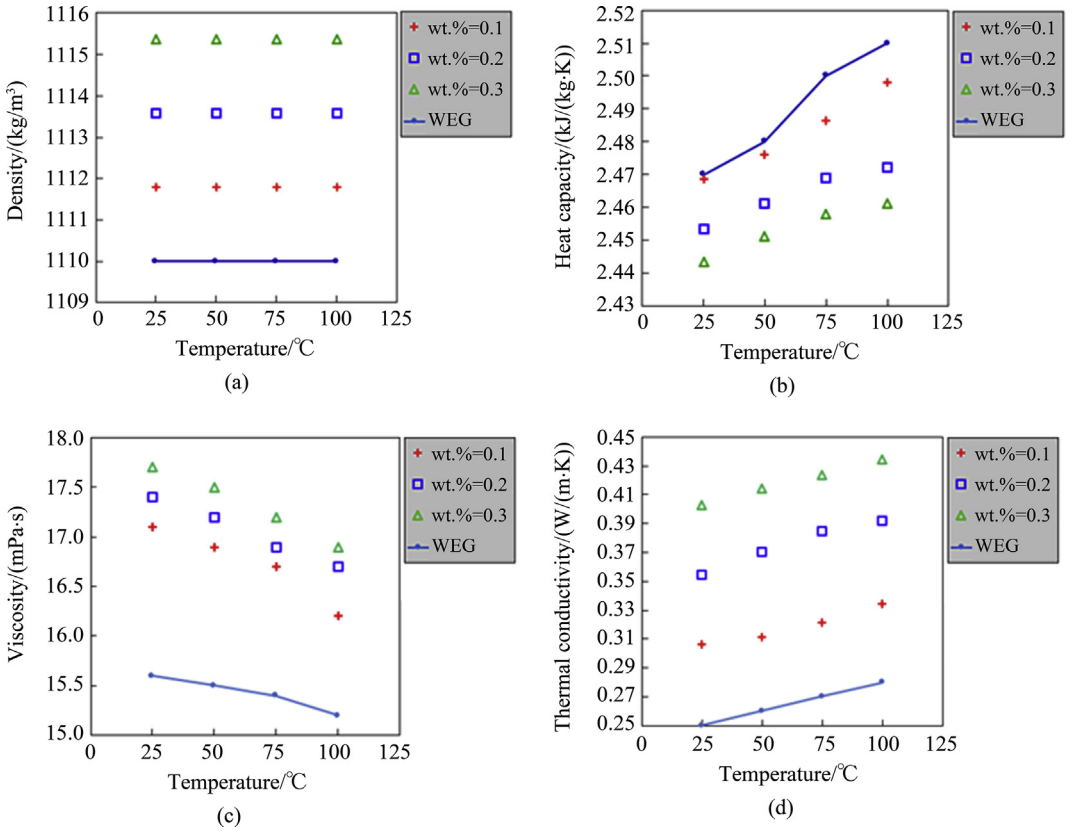

Figure 3 Thermo-physical properties of MgO/WEG NFs, (a) density, (b) heat capacity, (c) viscosity, and (d) thermal conductivity.

To calculate the FF of the system, following correlation was employed:

$$f = \frac{\Delta P}{\left(\frac{l}{d}\right) \times \frac{2 \times u^2}{\rho}} \tag{12}$$

here, f is the FF, ΔP is the FPD of the system. l is the total length of the HEX and d is the mean value for the tube diameter, u is the velocity of the heat transfer fluid (HTF). The

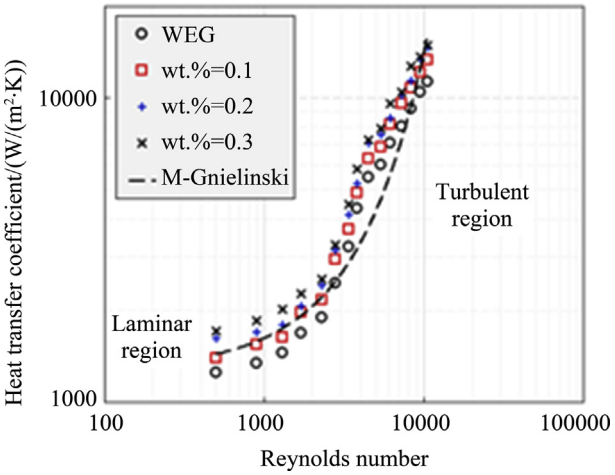

Figure 4 Dependence of HTC on Reynolds number at inlet temperature 50 °C.

uncertainty of the experiments was estimated with Kline-McKlintock [51] equation and the uncertainty of the HTC was 6.1%.

4. Result and discussion

4.1. Fluid flow

In Figure 4, variation of HTC with Reynolds number is depicted. To validate the results, the heat transfer coefficient measured for water/ethylene glycol was compared to the modified Gnielinski correlation which is well-known for turbulent fluid flow in tubes and pipes. As shown, a fair agreement is seen between the results and the correlation with ±13% deviation showing the reliability of the results for water. For water/ethylene glycol (WEG 50:50) at $Re = 500$, the HTC is 1255 W/(m^2·K), while it is 10,385 W/(m^2·K) at $Re = 9500$. Interestingly, by increasing the mass fraction of NF, the HTC increases. For an instance, for a given Reynolds number e.g. $Re = 3400$, at wt.% = 0.1, the HTC is 3702 W/(m^2·K), while it is 4127 W/(m^2·K) and 4469 W/(m^2·K), for wt.% = 0.2 and wt.% = 0.3, respectively. Importantly, the enhancement in HTC is attributed to the following reasons.

As previously shown, NPs intensifies the base fluid thermal conductivity. Brownian motion and thermophoresis are two main mechanisms involved in the enhancement of the HTC. When more NPs are within the base fluid, more

particle collision occurs within the base fluid resulting in the augmentation in Brownian motion and energy transport from one point in the base fluid to another point.

Presence of NPs within the thermal boundary layer reduces its thickness resulting in the enhancement of the HTC. One of the phenome involved in the enhancement of the HTC is the "thermophoresis phenomena" such that the NPs close to the hot region can receive thermal energy by conduction mechanism. By increasing the temperature of the particles, the kinetic energy is promoted and NPs move towards colder regions inside the liquid phase. Such a movement facilitate the transport of thermal energy and heat transfer in the HEX.

Figure 5 shows a schematic diagram of the above-mentioned plausible mechanisms. Notably, collision of NPs with each other within the base fluid changes the mean free path and also the direction of migration of NPs. Also, in a collision point, conduction heat transfer is the likely mechanism for the heat transfer between NPs.

In Figure 6, variation of the non-dimensional Nusselt number (*Nu*) with Reynolds number is depicted at different mass fractions of MgO NPs at 50 °C. As seen, Nusselt number lies within the range of 50−450 which has already been validated with the literature. Importantly, similar trends were seen for *Nu* number such that by increasing the FR and mass fraction of NF, the *Nu* number increases. The maximum enhancement for *Nu* number was 32.3% (in comparison with the base fluid). The enhancement for Nusselt number of NFs at wt.% = 0.1%, 0.2% and 0.3% (in comparison with the base fluid) was 15.9%, 26.2% and 32.3%, respectively at 50 °C. The highest *Nu* number was achieved at turbulent region, which was 432 at *Re* = 10,500.

4.2. Inlet temperature

In Figure 7, the change in HTC value at various Reynolds number is depicted. As shown, by increasing the inlet

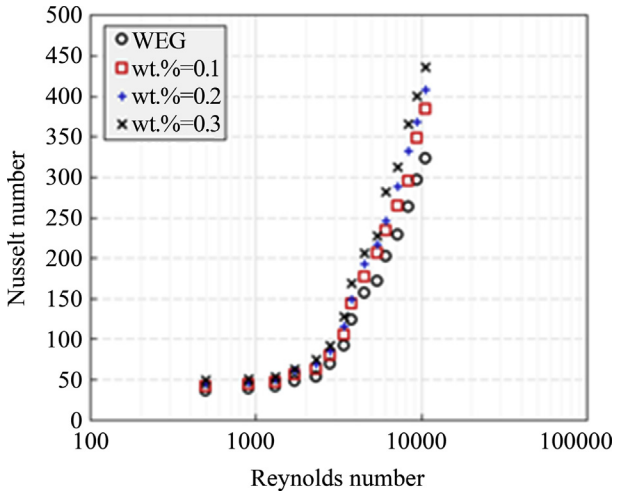

Figure 6 Variation of Nusselt number with Reynolds number at temperature of 50 °C.

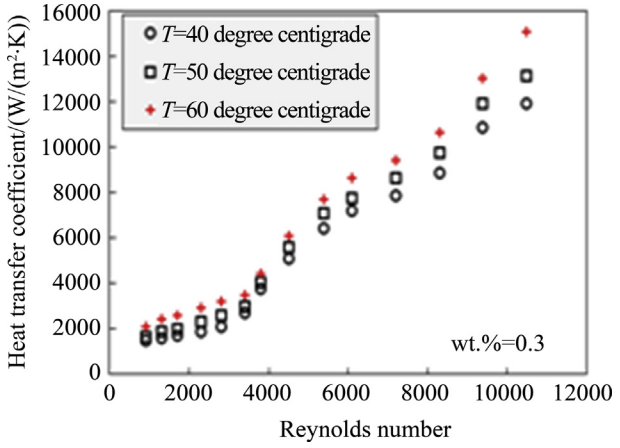

Figure 7 Variation of HTC at wt.% = 0.1 with Reynolds number for various temperatures.

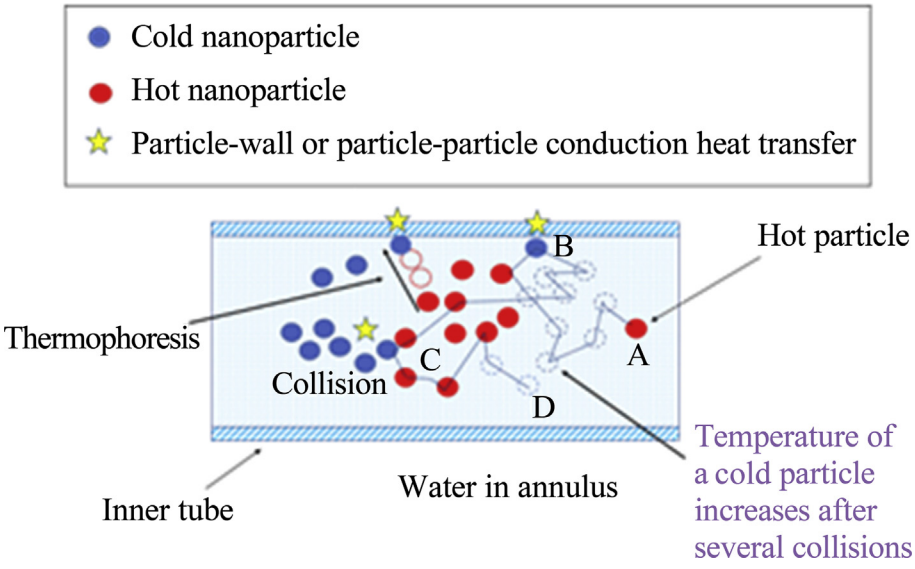

Figure 5 Illustration of the plausible mechanisms involved in the enhancement of the heat transfer in HEX.

temperature of the NF, higher HTC value was recorded. This is because temperature of NF can promote some of the physical properties such as thermal conductivity. However, this is not significant in the laminar region and the maximum enhancement of HTC in this region was 6.5%. However, for turbulent region, the enhancement was pronounced up to 18.7%. Notably, the temperature was increased in a way that the NF remain in the single-phase at all times and flow conditions. Moreover, according to the literature [52,53], Brownian motion and thermophoresis, both are intensified with the increase in temperature of NF, which is in accordance with the results obtained in the present research.

4.3. Fluid pressure drop

Figure 8 presents the dependence of FPD on Reynolds number for different NFs. As can be seen, for the base fluid, by increasing the Reynolds number, the FPD value increases. For example, at $Re = 500$, the FPD value for water/ethylene glycol is 11 kPa, while at $Re = 3400$ and $Re = 10{,}500$, it is 55 kPa and 143 kPa, respectively. The maximum enhancement for the FPD value is 1200%, which is largely due to the small diameter of the tube. Interestingly, presence of the MgO NPs within the base fluid augments the FPD value at any mass fractions. For example, at a given $Re = 1700$, at wt.% = 0.1, the FPD is 28 kPa, while it is 36 kPa at wt.% = 0.2 and at the same Reynolds number. This is because, presence of NPs increases the friction forces and shear between the layers of the base fluid in NF, resulting in the increase in the viscosity of NF. Since FPD is a strong function of the viscosity, thereby higher viscosity means higher FPD value. Therefore, when it comes to the influence of mass fraction of NF, it can be stated that there is a penalty for the FPD and consequently, there is a trade-off behaviour between the mass fraction of NPs and the enhancement in the FPD. The higher, the mass fraction of NPs is, the higher the thermal conductivity, HTC and also the higher value for the FPD is registered. This trend is seen for all the inlet temperatures. Noticeably, the value for the

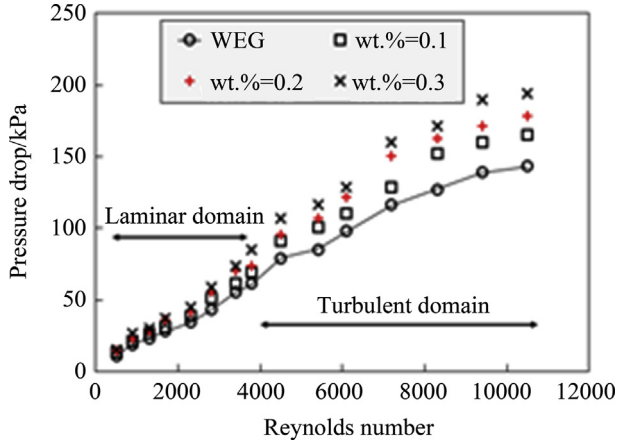

Figure 8 Effect of the Reynolds number on the value of the FPD.

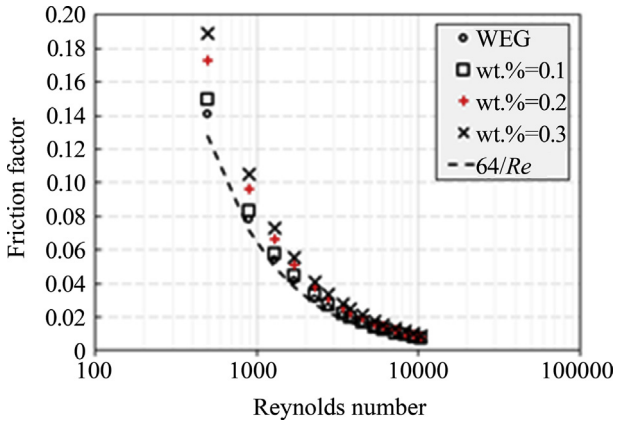

Figure 9 Effect of Reynolds number on FF value and a comparison against equation of "64/*Re*" extracted from the literature [54].

FPD in laminar region is considerably lower than that of registered in the turbulent region, which is largely due to the formation of eddies, intensification of Brownian motion and particle collision in turbulent regime. Regardless of the NP's mass fraction, the FPD value for all the NFs was higher than that of registered for the WEG base fluid.

4.4. Friction factor

Influence of NPs on the FPD is a clear sign for its influence on the FF. In Figure 9, variation of the FF value with Reynolds number is depicted. For validating the results, Darcy formula was utilized for BOTH laminar and turbulent regions. The trend seen for the FF value was found to follow the Darcy equation, which in turn shows that the FF measured for the WEG and NFs is reasonably valid. Also, by increasing the FR of flow, the FF decreases. Interestingly, by increasing the mass fraction of NF, the FF increases. This is also due to the enhancement in the viscosity of NF. Moreover, presence of NPs within the layers of the base fluid increases the friction forces between particle-fluid, particle-particle and particle-wall of the HEX. The maximum augmentation for the FF was recorded at wt.% = 0.3 by 33.8% over that of registered for WEG. Notably, reduction in the FF with Reynolds number showed

Table 3 Well-known correlations used in the present research to estimate the heat transfer coefficient against the experimental data [2].

Correlation	Author	Correlation	A.A.D /%
Corr. 1	Pantzali et al. [55]	$Nu = 0.247 \times Re^{0.66} \times Pr^{0.3}$	14.2
Corr. 2	Huang et al. [56]	$Nu = 0.3762 \times Re^{0.6681} \times Pr^{0.3}$	28.7
Corr. 3	Rabienataj et al. [57]	$Nu = 1.25 \times (Re - 1500)^{0.357} \times Pr^{0.07} \times (1 + 2.5 \times \varphi^{0.54})$	19.1

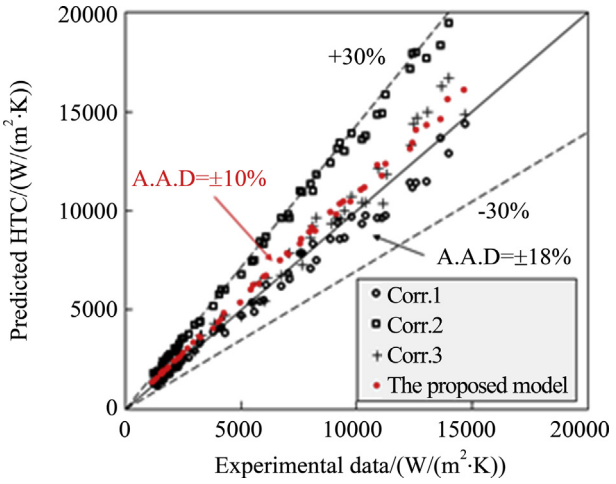

Figure 10 A rough comparison between the predicted HTC and the experimental HTC.

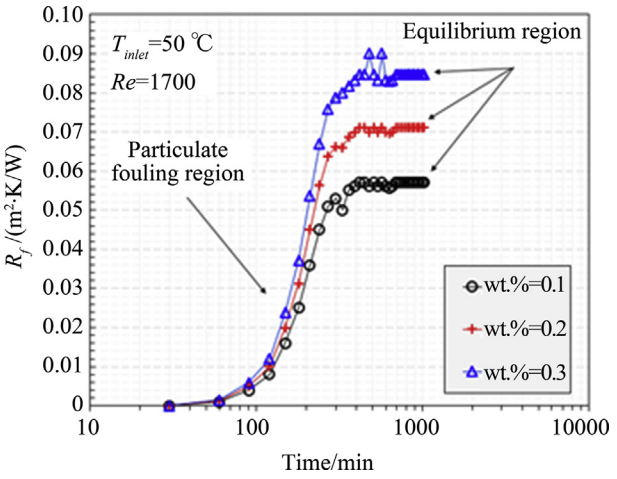

Figure 11 Dependence of fouling thermal resistance on time of the experiments for different NFs.

a nonlinear relationship and also the maximum reduction was seen in turbulent heat transfer regime.

4.5. Correlation of experimental data

To validate and to correlate the experimental data gathered for the heat transfer coefficient, first the data were examined against three well-known correlations given in Table 3.

Figure 10 presents the comparison between the results obtained with the above correlations and those of experimentally measured. As can be seen, the results predicted with the correlations are in a fair agreement with the experimental data within the 30% and 20%, respectively.

This significant difference between the correlations and the experimental data is largely due to the considerable change in thermo-physical properties of the water/ethylene glycol due to the presence of MgO nanoparticles. Thereby, for better estimation of the heat transfer coefficient, with the help of regression analysis and dimensional analysis, a new correlation was developed to predict the Nusselt number, which is presented in the following correlation:

$$Nu = 0.3722 \times Re^{0.631} \times Pr^{0.29} \quad (13)$$

here, *Re*, *Pr* are Reynolds and Prandtl numbers, respectively. As can be seen in Figure 9, the correlation enables one to estimate the Nusselt number for MgO/water-ethylene glycol with the reasonable accuracy of 10% against the experimental data and other correlations. Notably, for *Re* and *Pr* numbers, the thermo-physical properties of NF should be used. For the present research, the experimental thermo-physical properties were used, which resulted in a reasonable accuracy of the equation.

Due to the interaction of NPs with the base fluid and also walls of the HEX together with temperature difference within the base fluid, particles can lose their stability and stick to the walls of the HEX. This phenomenon is referred to as particulate fouling. In particulate fouling, time is the key parameter and the determining factor. Time can determine whether or not nanoparticles form the fouling layer on the surface. Also, there are two other main parameters influencing the rate of fouling namely mass fraction of NPs and FR of the nano-suspension.

4.6. Particulate fouling

Figure 11 represents the dependence of fouling thermal resistance on time of the experiments for various mass fraction of NPs. By increasing the mass fraction of the NPs, the fouling thermal resistance parameter increases. R_f follows an asymptotic trend with time. It means that at initial time of the experiment, the fouling resistance is relatively small in comparison with other times. Then, with an increase in time, fouling thermal resistance dramatically increases reaching to a point in which R_f does not change with time. This is because at first, there is no NPs on the surface and stickability of surface for NPs on walls is very small since fluid flow velocity vector on the walls is very small (approximately equals to zero). Therefore, NPs are exposed to a small kinetic energy coming from the base fluid. Thereby, due to the roughness and irregularity of surface, NPs stick to the wall of the heat exchanger. However, with an increase in time, more NPs attach to the surface creating a porous layer of fouling on the wall. With time, the thickness of the fouling increases and the outer layer of NPs are exposed to the fluid flow with higher velocity vector, resulting in the removal of the NPs from the fouling layer. Therefore, fouling formation reaches to an equilibrium in which the rate of particle deposition on wall equals to the particle removal from the fouling layer (equilibrium region), which has been shown in Figure 10.

Figure 12 shows the variation of fouling thermal resistance with time at different Reynold numbers. As can be seen, at lower Reynolds numbers, the fouling thermal resistance is lower and with an increase in flow rate of NF,

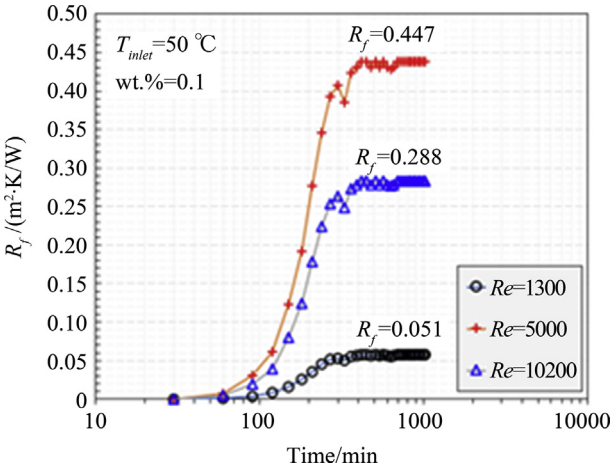

Figure 12 Dependence of fouling thermal resistance on time of the experiments for different FRs.

the fouling thermal resistance increases. For example, for wt.% = 0.1, the fouling thermal resistance reaches the equilibrium region with the value of 0.051 $(m^2 \cdot K)/W$. Likewise, the same trend is seen at other *Re* numbers. However, at *Re* = 5000, the highest fouling thermal resistance was observed which is 0.447 $(m^2 \cdot K)/W$. Again, by increasing the Reynolds number, the fouling thermal resistance of the system decreases. This is because at higher *Re* numbers, the velocity vector close to the wall is sufficient for removing the particulate fouling layer of the nanoparticles. Therefore, there is a point in which role of fluid flow (fluid velocity) changes from deposition flow flux to removal flow flux. It is highly-recommended to conduct further research to understand the exact behaviour of particulate fouling and develop the knowledge and know-how behind the particulate fouling of the nanoparticles. This will be a step-change and a game changer in commercialization of the nanofluids for high-temperature applications.

4.7. Thermal performance index

To further clarify the trade-off between the heat transfer enhancement and the pressure drop penalty due to the presence of nanoparticles within the base fluid, a new parameter is defined as follows [58–61]:

$$PI = \frac{Nu_{nf}}{Nu_{bf}} \times \left(\frac{\Delta p_{bf}}{\Delta p_{nf}}\right)^{0.33} \quad (14)$$

nf and *bf* stand for nanofluid and the base fluid, respectively and *Nu* is the Nusselt number. Figure 13 presents the dependence of thermal performance index on Reynolds number and mass fractions of nanofluid. As can be seen, despite the trade-off trend between the influence of mass fraction of nanofluid on heat transfer enhancement and penalty for pressure drop, still thermal performance index increases with an increase in the mass fraction of nanofluid. This is because, the rate of enhancement in heat transfer coefficient is several times higher than increase in the pressure drop value resulting in the total increase of the thermal performance index. Thereby, with some reservations, it can be concluded that presence of NPs can plausibly increase the heat transfer coefficient within the heat exchanger. However, detailed assessment of the pumping power is still required to draw the final conclusion, which is beyond the scope of the present work.

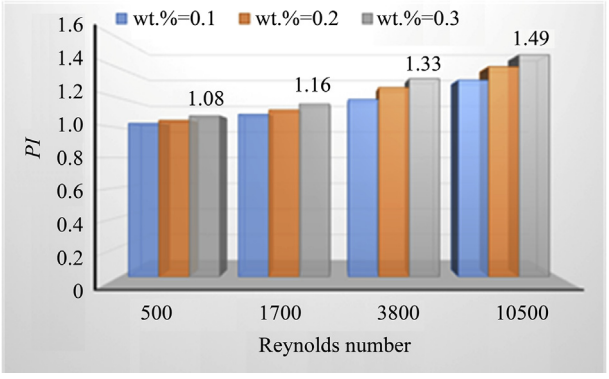

Figure 13 Effect of Reynolds number on PI value at different mass fractions of MgO NPs.

5. Conclusion

In light of above discussions, following conclusions were drawn:

(1) Mass concentration of NF promoted the HTC value of the HEX considerably. The largest recorded enhancement was 39% at wt.% = 0.3, which was associated with two micro-scale mechanisms of Brownian motion and thermophoresis.
(2) The inlet temperature slightly enhanced some of the physical properties of NF. Which led to the slight increase in the HTC value.
(3) FPD of and FF of the system were augmented by increasing the mass fraction of the NPs in the liquid phase. For any tests, the NPs augmented the FPD and FF values when comparing to the base fluid. This was because of the enhancement in the viscosity of NF and friction forces due to the enhancement in the friction between the layers of the fluid.
(4) The existing correlation failed to accurately estimate the HTC. Thereby, using a regression analysis, a new equation was developed which estimates the HTC for MgO-water-ethylene glycol with accuracy of ±10%. Note that the applicability of this model against other NFs need to be researched.
(5) Investigating the PI value of the system showed that despite the increase in FPD and FF values, the PI value was still plausible showing that MgO/WEG NFs can be a potential coolant for thermal engineering systems.

Acknowledgement

Authors of this work tend to appreciate the University of Adelaide for sharing the scientific facilities and micro-fluidics laboratory.

References

[1] M. Sarafraz, F. Hormozi, S. Peyghambarzadeh, N. Vaeli, Upward flow boiling to DI-water and CuO nanofluids inside the concentric annuli, J. Appl. Fluid Mech. 8 (2015) 651−659.
[2] D.S. Weaver, J.A. Fitzpatrick, A review of cross-flow induced vibrations in heat exchanger tube arrays, J. Fluid Struct. 2 (1) (1988) 73−93.
[3] M. Bahiraei, R. Rahmani, A. Yaghoobi, E. Khodabandeh, R. Mashayekhi, M. Amani, Recent research contributions concerning use of nanofluids in heat exchangers: a critical review, Appl. Therm. Eng. 133 (2018) 137−159.
[4] M.L.R. Chaitanya Lahari, P.H.V. Sesha Talpa Sai, K.S. Narayana Swamy, N. Krishnamurthy, K.V. Sharma, Investigation on heat transfer properties of water based TiO_2-ZnO nanofluids, IOP Conference Series: Materials Science and Engineering 455 (2018) 012092.
[5] R. Daghigh, P. Zandi, Experimental analysis of heat transfer in spiral coils using nanofluids and coil geometry change in a solar system, Appl. Therm. Eng. 145 (2018) 295−304.
[6] L. Ghalib, N.M. Rahma, K.M. Eweed, A.K. Al-Kamal, Flow and heat transfer experimental investigation of nanofluid in a double pipe heat exchanger, IOP Conference Series: Materials Science and Engineering 454 (2018) 012150.
[7] M. Sheikholeslami, M. Jafaryar, A. Shafee, Z. Li, Nanofluid heat transfer and entropy generation through a heat exchanger considering a new turbulator and CuO nanoparticles, J. Therm. Anal. Calorim. 134 (2018) 2295−2303.
[8] I. Tayyab Ul, R. Tariq, K.A. Sheikh, M. Shayyan, Study of thermal performance of common heat exchangers by using nanofluids, in: ICAEM 2018 - 2018 International Conference on Applied and Engineering Mathematics, 2018, pp. 130−135.
[9] R. Ul Haq, F.A. Soomro, Z. Hammouch, S. Ur Rehman, Heat exchange within the partially heated C-shape cavity filled with the water based SWCNTs, Int. J. Heat Mass Tran. 127 (2018) 506−514.
[10] Z. Wang, Z. Wu, B. Sundén, Effects of graphene ethylene glycol/water nanofluids on the performance of a brazed plate heat exchanger, J Nanofluids 7 (2018) 1069−1074.
[11] M.M.A. Bhutta, N. Hayat, M.H. Bashir, A.R. Khan, K.N. Ahmad, S. Khan, CFD applications in various heat exchangers design: a review, Appl. Therm. Eng. 32 (2012) 1−12.
[12] A. Mueller, J. Chiou, Review of various types of flow maldistribution in heat exchangers, Heat Tran. Eng. 9 (1988) 36−50.
[13] G.F. Hewitt, G.L. Shires, T.R. Bott, Process Heat Transfer, CRC Press, Boca Raton, FL, 1994.
[14] S. Kakac, H.T. Liu, A. Pramuanjaroenkij, Heat Exchangers: Selection, Rating, and Thermal Design, CRC Press, 2012.
[15] S. Kakaç, A. Pramuanjaroenkij, Review of convective heat transfer enhancement with nanofluids, Int. J. Heat Mass Tran. 52 (2009) 3187−3196.
[16] G. Huminic, A. Huminic, Hybrid nanofluids for heat transfer applications − a state-of-the-art review, Int. J. Heat Mass Tran. 125 (2018) 82−103.
[17] M.E. Nakhchi, J.A. Esfahani, Cu-water nanofluid flow and heat transfer in a heat exchanger tube equipped with cross-cut twisted tape, Powder Technol. 339 (2018) 985−994.
[18] B. Raei, S.M. Peyghambarzadeh, R. Salehi Asl, Experimental investigation on heat transfer and flow resistance of drag-reducing alumina nanofluid in a fin-and-tube heat exchanger, Appl. Therm. Eng. 144 (2018) 926−936.
[19] M. Sivahari Shankar, P. Immanuel, M. Eswaran, Heat transfer analysis of shell and tube heat exchanger using Al_2O_3 nanofluids, Int. J. Mech. Eng. Technol. 9 (2018) 980−989.
[20] S.K. Vandrangi, S. Emani, G. Velidi, K.V. Sharma, Friction factor analysis of SiO_2 and Al_2O_3 nanofluids dispersed in 60 EGW and 40 EGW base fluids, J Adv Res Fluid Mech Therm Sci 51 (2018) 61−70.
[21] M. Elias, I. Mahbubul, R. Saidur, M. Sohel, I. Shahrul, S. Khaleduzzaman, S. Sadeghipour, Experimental investigation on the thermo-physical properties of Al_2O_3 nanoparticles suspended in car radiator coolant, Int. Commun. Heat Mass Tran. 54 (2014) 48−53.
[22] V. Trisaksri, S. Wongwises, Critical review of heat transfer characteristics of nanofluids, Renew. Sustain. Energy Rev. 11 (2007) 512−523.
[23] M. Biglarian, M.R. Gorji, O. Pourmehran, G. Domairry, H_2O based different nanofluids with unsteady condition and an external magnetic field on permeable channel heat transfer, Int. J. Hydrogen Energy 42 (2017) 22005−22014.
[24] M. Mohammadian, O. Pourmehran, P. Ju, An iterative approach to obtaining the nonlinear frequency of a conservative oscillator with strong nonlinearities, Int. Appl. Mech. 54 (2018) 470−479.
[25] O. Pourmehran, M. Rahimi-Gorji, D.D. Ganji, Analysis of nanofluid flow in a porous media rotating system between two permeable sheets considering thermophoretic and brownian motion, Therm. Sci. 21 (5) (2017) 2057−2067.
[26] O. Pourmehran, M. Rahimi-Gorji, M. Gorji-Bandpy, M. Baou, Comparison between the volumetric flow rate and pressure distribution for different kinds of sliding thrust bearing, Propul Power Res 4 (2015) 84−90.
[27] O. Pourmehran, M. Sarafraz, M. Rahimi-Gorji, D. Ganji, Rheological behaviour of various metal-based nano-fluids between rotating discs: a new insight, J Taiwan Inst Chem Eng 88 (2018) 37−48.
[28] N. Vakili, M. Nakhjavani, H. Mirzayi, F. Shirazi, Studying silibinin effect on human endothelial and hepatocarcinoma cell lines, J Res Pharmaceut Sci 7 (2012) 174.
[29] F.H. Shirazi, A. Zarghi, F. Kobarfard, R. Zendehdel, M. Nakhjavani, S. Arfaiee, T. Zebardast, S. Mohebi, N. Anjidani, A. Ashtarinezhad, Remarks in successful cellular investigations for fighting breast cancer using novel synthetic compounds, in: Breast Cancer-Focusing Tumor Microenvironment, Stem Cells and Metastasis, InTech, 2011.
[30] Z.J. Luan, G.M. Zhang, M.C. Tian, M.X. Fan, Flow resistance and heat transfer characteristics of a new-type plate heat exchanger, J Hydrodyn, Ser. B 20 (2008) 524−529.
[31] S. Lee, Y. Cho, C. Bai, D. Cho, The effect of aspect ratio on turbulent flow heat transfer and pressure drop in a plate heat exchanger, Int. J. Heat Exch. 1 (2000) 113−124.
[32] S. Peyghambarzadeh, S. Hashemabadi, M.S. Jamnani, S. Hoseini, Improving the cooling performance of automobile radiator with Al_2O_3/water nanofluid, Appl. Therm. Eng. 31 (2011) 1833−1838.
[33] S. Peyghambarzadeh, S. Hashemabadi, S. Hoseini, M.S. Jamnani, Experimental study of heat transfer enhancement using water/ethylene glycol based nanofluids as a new coolant for car radiators, Int. Commun. Heat Mass Tran. 38 (2011) 1283−1290.
[34] S. Peyghambarzadeh, S. Hashemabadi, M. Naraki, Y. Vermahmoudi, Experimental study of overall heat transfer coefficient in the application of dilute nanofluids in the car radiator, Appl. Therm. Eng. 52 (2013) 8−16.
[35] A. Bhattad, J. Sarkar, P. Ghosh, Discrete phase numerical model and experimental study of hybrid nanofluid heat transfer and pressure drop in plate heat exchanger, Int. Commun. Heat Mass Tran. 91 (2018) 262−273.
[36] B.A.K. Naik, A.V. Vinod, Heat transfer enhancement using non-Newtonian nanofluids in a shell and helical coil heat exchanger, Exp. Therm. Fluid Sci. 90 (2018) 132−142.
[37] V. Kumar, A.K. Tiwari, S.K. Ghosh, Characterization and performance of nanofluids in plate heat exchanger, Mater. Today: Proc 4 (2017) 4070−4078.
[38] K. Anoop, J. Cox, R. Sadr, Thermal evaluation of nanofluids in heat exchangers, Int. Commun. Heat Mass Tran. 49 (2013) 5−9.

[39] B.-H. Chun, H.U. Kang, S.H. Kim, Effect of alumina nanoparticles in the fluid on heat transfer in double-pipe heat exchanger system, Kor. J. Chem. Eng. 25 (2008) 966−971.
[40] A. Zamzamian, S.N. Oskouie, A. Doosthoseini, A. Joneidi, M. Pazouki, Experimental investigation of forced convective heat transfer coefficient in nanofluids of Al_2O_3/EG and CuO/EG in a double pipe and plate heat exchangers under turbulent flow, Exp. Therm. Fluid Sci. 35 (2011) 495−502.
[41] R.S. Khedkar, S.S. Sonawane, K.L. Wasewar, Heat transfer study on concentric tube heat exchanger using TiO_2−water based nanofluid, Int. Commun. Heat Mass Tran. 57 (2014) 163−169.
[42] M. Akhtari, M. Haghshenasfard, M. Talaie, Numerical and experimental investigation of heat transfer of α-Al_2O_3/water nanofluid in double pipe and shell and tube heat exchangers, Numer. Heat Tran., Part A: Applications 63 (2013) 941−958.
[43] M.S. Dehaj, M.Z. Mohiabadi, Experimental investigation of heat pipe solar collector using MgO nanofluids, Sol. Energy Mater. Sol. Cell. 191 (2019) 91−99.
[44] H. Khodadadi, D. Toghraie, A. Karimipour, Effects of nanoparticles to present a statistical model for the viscosity of MgO-water nanofluid, Powder Technol. 342 (2019) 166−180.
[45] A. Asadi, F. Pourfattah, Heat transfer performance of two oil-based nanofluids containing ZnO and MgO nanoparticles; a comparative experimental investigation, Powder Technol. 343 (2019) 296−308.
[46] M.H. Esfe, H. Rostamian, A. Shabani-samghabadi, A.A.A. Arani, Application of three-level general factorial design approach for thermal conductivity of MgO/water nanofluids, Appl. Therm. Eng. 127 (2017) 1194−1199.
[47] M.H. Ahmadi, A. Mirlohi, M.A. Nazari, R. Ghasempour, A review of thermal conductivity of various nanofluids, J. Mol. Liq. 265 (2018) 181−188.
[48] G. Ramesh, N.K. Prabhu, Review of thermo-physical properties, wetting and heat transfer characteristics of nanofluids and their applicability in industrial quench heat treatment, Nanoscale Res Lett 6 (2011) 334.
[49] W. Azmi, K. Sharma, R. Mamat, A. Alias, I.I. Misnon, Correlations for thermal conductivity and viscosity of water based nanofluids, in: IOP Conference Series: Materials Science and Engineering Vol. 36, IOP Publishing, 2012, pp. 012029.
[50] M.M. Sarafraz, M. Arjomandi, Thermal performance analysis of a microchannel heat sink cooling with copper oxide-indium (CuO/In) nano-suspensions at high-temperatures, Appl. Therm. Eng. 137 (2018) 700−709.
[51] S.J. Kline, F.A. McClintock, Describing uncertainties in single-sample experiments, ASME Mech Eng 75 (1953) 3−8.
[52] S.P. Jang, S.U. Choi, Role of Brownian motion in the enhanced thermal conductivity of nanofluids, Appl. Phys. Lett. 84 (2004) 4316−4318.
[53] P. Shima, J. Philip, B. Raj, Role of microconvection induced by Brownian motion of nanoparticles in the enhanced thermal conductivity of stable nanofluids, Appl. Phys. Lett. 94 (2009) 223101.
[54] W.L. Hogarth, J.-Y. Parlange, C.W. Rose, C. Fuentes, R. Haverkamp, M.T. Walter, Interpolation between Darcy-Weisbach and Darcy for laminar and turbulent flows, Adv. Water Resour. 28 (2005) 1028−1031.
[55] M. Pantzali, A. Mouza, S. Paras, Investigating the efficacy of nanofluids as coolants in plate heat exchangers (PHE), Chem. Eng. Sci. 64 (2009) 3290−3300.
[56] D. Huang, Z. Wu, B. Sundén, Pressure drop and convective heat transfer of Al_2O_3/water and MWCNT/water nanofluids in a chevron plate heat exchanger, Int. J. Heat Mass Tran. 89 (2015) 620−626.
[57] A.R. Darzi, M. Farhadi, K. Sedighi, Heat transfer and flow characteristics of Al_2O_3-water nanofluid in a double tube heat exchanger, Int. Commun. Heat Mass Tran. 47 (2013) 105−112.
[58] M. Omidi, M. Farhadi, M. Jafari, A comprehensive review on double pipe heat exchangers, Appl. Therm. Eng. 110 (2017) 1075−1090.
[59] A. Kumar, A. Layek, Thermo-hydraulic performance of solar air heater having twisted rib over the absorber plate, Int. J. Therm. Sci. 133 (2018) 181−195.
[60] R. Webb, E. Eckert, R. Goldstein, Generalized heat transfer and friction correlations for tubes with repeated-rib roughness, Int. J. Heat Mass Tran. 15 (1972) 180−184.
[61] S.K. Samal, M.K. Moharana, Thermo-hydraulic performance evaluation of a novel design recharging microchannel, Int. J. Therm. Sci. 135 (2019) 459−470.